Available online at www.sciencedirect.com
ScienceDirect
Organic Electronics 8 (2007) 505–512
Organic Electronics
www.elsevier.com/locate/orgel

Growth enhancement and field emission characteristics of one-dimensional 3,4,9,10-perylenetetracarboxylic dianhydride nanostructures on pillared titanium substrate

Shich-Chang Suen [a], Wha-Tzong Whang [a,*], Fu-Ju Hou [b], Bau-Tong Dai [b]

[a] *Department of Materials Science and Engineering, National Chiao Tung University, 1001 Ta Hsueh Road, Hsinchu 30050, Taiwan, ROC*
[b] *National Nano Device Laboratories, No. 26, Prosperity Road I, Science-based Industrial Park, Hsinchu, Taiwan, ROC*

Received 8 January 2007; received in revised form 7 March 2007; accepted 12 March 2007
Available online 19 March 2007

Abstract

We have utilized the π–π interactions between 3,4,9,10-perylenetetracarboxylic dianhydride (PTCDA) molecules and temperature-induced morphology changes to synthesize one-dimensional (1D) nanostructures of PTCDA on a heated (ca. 100 °C) titanium substrate through vacuum sublimation. Because of the pillared Ti structures and the presence of reactive Ti–Cl sites, the titanium substrate played a crucial role in assisting the PTCDA molecules to form 1D nanostructures. The average diameter of the nanofibers deposited on the Ti-CVD substrate, a Ti substrate formed by chemical vapor deposition (CVD), at 100 °C was ca. 84 nm, with lengths ranging from 100 nm to 3 μm. When the PTCDA nanofibers were biased under vacuum, the emission current remained stable. The turn-on electric field for producing a current density of 10 $\mu A/cm^2$ was 8 V/μm. The maximum emission current density was 1.3 mA/cm^2, measured at 1100 V ($E = 11$ V/μm). From the slope of the straight line obtained after plotting $\ln(J/E^2)$ versus $1/E$, we calculated the field enhancement factor β to be ca. 989. These results demonstrate the PTCDA nanofibers have great potential for applicability in organic electron-emitting devices.

PACS: 79.70.+q; 81.07.Nb; 85.35; 81.16.Dn; 72.80.Le

Keywords: PTCDA; Nanofibers; Field Emission; Morphology; Pillared titanium

1. Introduction

3,4,9,10-Perylenetetracarboxylic dianhydride (PTCDA) is one of the most intensively studied materials for organic electronic and optoelectonic applications [1,2]. Investigations into its bulk properties, such as its photoconductivity [3], carrier transport [4], and electroluminescence [5], have led to PTCDA's rapid development for applications in light emitting devices [6], field effect transistors [7], and solar cells [8]. Recently, a number of π-stacking organic molecules, including tris(8-hydroxyquinoine)aluminum [9], (7,7,8,8-tetracyanoquinodimethane)silver [10], coronene [11], anthracene [12], perylene [12], and copper phthalocyanine (CuPc)

* Corresponding author. Tel.: +886 3 5726111x31873; fax: +886 3 5724727.
E-mail address: wtwhang@mail.NCTU.edu.tw (W.-T. Whang).

1566-1199/$ - see front matter © 2007 Elsevier B.V. All rights reserved.
doi:10.1016/j.orgel.2007.03.003

[13], have been demonstrated to form one-dimensional (1D) nanostructures readily under milder conditions than those used typically to prepare analogous structures from inorganic compounds. Moreover, most of these organic 1D nanostructures possess excellent field emission characteristics when biased in a vacuum chamber. Because the morphology of planar π-stacked PTCDA molecules on various substrates can be altered through modification of the processing temperature – i.e., granular morphologies at room temperature, island morphologies at high temperature [14–19] – we suspected that PTCDA might form 1D structures under certain conditions. In this paper, we present nanofibers having high aspect ratios formed using a relatively low-temperature (100 °C) process and describe the significant effect that the Ti substrate formed by plasma enhancement chemical vapor deposition (PECVD) has on the 1D structural growth. We also evaluate the field emission characteristics of the PTCDA nanofibers synthesized directly on Ti metal films. The results open up an interesting area of study and suggest potential further applications.

2. Experimental procedure

PTCDA films were grown through vacuum sublimation in a thermal coater at a base pressure of ca. 3×10^{-6} torr. A commercial powder of PTCDA (Aldrich) was sublimed onto various substrates, including Ti and Au, from a heated crucible. The crucible temperature of ca. 100 °C corresponded to a deposition rate of 1 Å/s, as determined using a quartz crystal microbalance. To study the effect that altering the temperature had on the film morphology, the substrate temperature (T_{sub}) was maintained at 25, 80, 100, or 120 °C. The Au substrate was prepared by depositing an Au film on a Si (100) substrate through electron-beam gun evaporation (physical vapor deposition; PVD). We denote this substrate as "Au-PVD". The Ti substrate was prepared by depositing a Ti film on a Si (100) substrate using the PECVD technique. This sample is denoted as "Ti-CVD". Details of the PECVD process have been reported elsewhere [20]. It mainly utilizes titanium tetrachloride ($TiCl_4$) to react with H_2 and form a metallic Ti film in a plasma-generating chamber. A Ti substrate deposited using the sputter technique (a variation on PVD) was also prepared to ascertain the effect that the substrate has on forming the PTCDA nanofibers. We denote this substrate as "Ti-PVD".

Structural investigations were performed using a JEOL JSM-6500F scanning electron microscope (SEM). The profiles and fine structures of the nanostructures were imaged and analyzed using a JEOL JEM-2010F high-resolution transmission electron microscope (HRTEM) equipped with an Oxford energy dispersive spectrometer. The substrate morphologies were investigated using a Veeco D5000 atomic force microscope (AFM). The concentration of trace elements was determined using an ATOMIKA TXRF-8030W total reflection X-ray fluorescence (TXRF) spectrometer. The field emission measurements were performed in a vacuum chamber (ca. 10^{-6} torr) where a cylindrical copper electrode (diameter: 2.2 mm) was positioned above the sample surface at a distance of 100 μm. A Keithley 237 instrument was used to measure the emission current of the PTCDA nanofibers as a function of the sweep bias.

3. Results and discussion

PTCDA molecules tend to form island morphologies on various substrates at elevated temperatures [14–19]. To determine the growth conditions necessary to prepare PTCDA nanofibers, we deposited PTCDA onto Ti and Au substrates at various temperatures and assessed the film morphologies by means of SEM.

Figs. 1a–h display SEM topographic images of PTCDA films deposited on Au and Ti-CVD substrates under various temperatures. At room temperature, the film morphology on the Au substrate was that of contiguous granular structures having an average grain size of 45 nm (Fig. 1a). As the substrate temperature increased, we observed typical temperature-induced morphological changes [19,21]; i.e., Figs. 1b–d indicate that the film morphologies changed from grains to facets and finally to separated islands upon increasing the temperature. According to Krause et al., PTCDA films deposited at room temperature are metastable. When PTCDA is deposited at elevated temperatures, or when PTCDA-coated substrates are annealed at high temperatures, the adsorbate contains a sufficient amount of energy to diffuse to already existing crystallite sites in an energetically favorable process [14,15]. Such morphological changes may also occur through strain relaxation mechanisms [21]. As a result of strong chemisorption, the first layer of PTCDA is strained, such that the molecules adsorbed onto larger island sites have

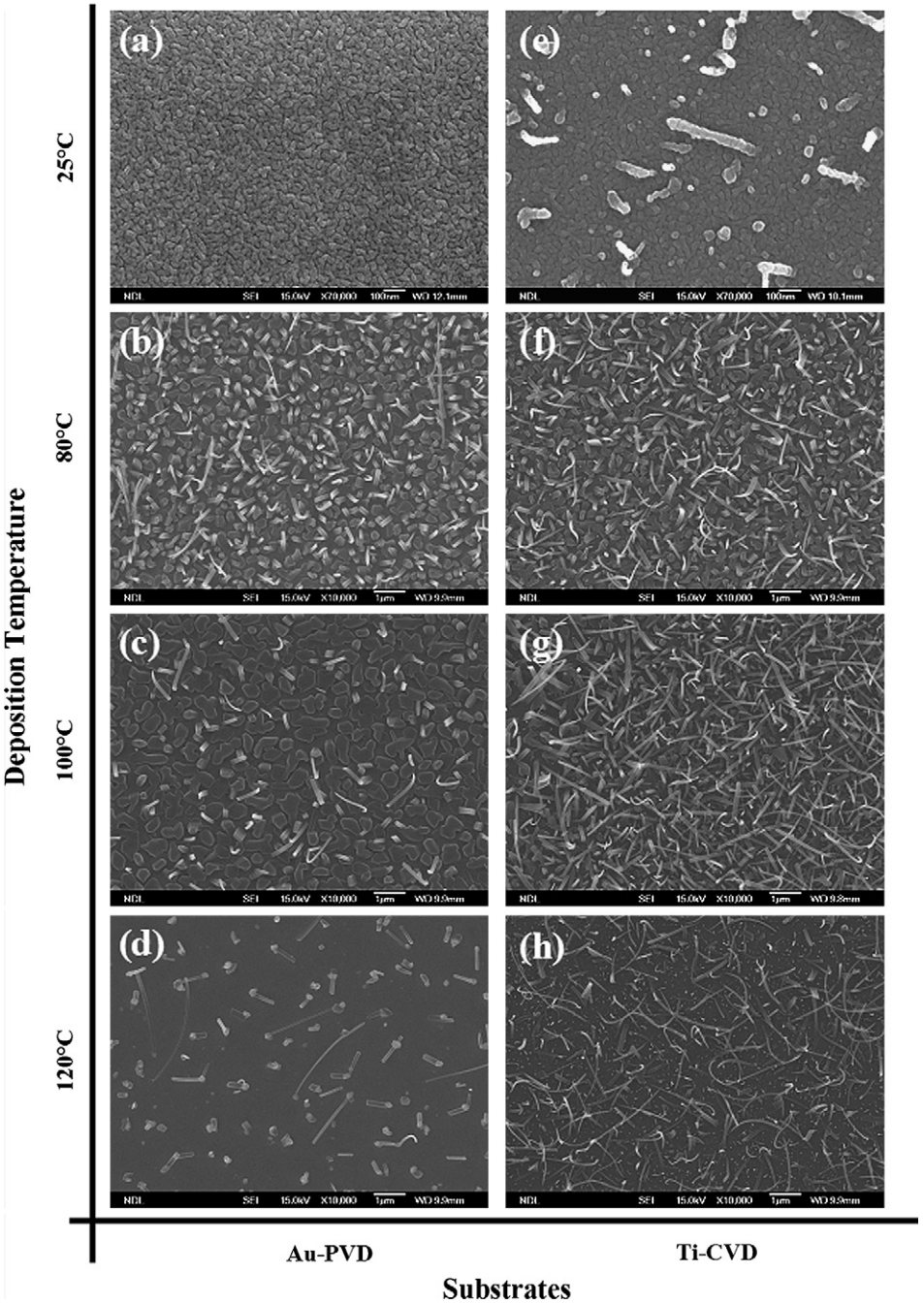

Fig. 1. Top-view SEM images of PTCDA layers deposited on an Au substrate at values of T_{sub} of (a) 25, (b) 80, (c) 100, and (d) 120 °C and on a Ti substrate at values of T_{sub} of (e) 25, (f) 80, (g) 100, and (h) 120 °C. To discern the subtle difference between samples deposited at room temperature, the images of (a) and (e) have been magnified by 70,000 times, whereas the others have been magnified only 10,000 times.

lower energies than those adsorbed onto smaller island sites, and therefore Stranski–Krastanov (SK) growth help to relax this strain [18,22]. When the temperature increases, the islands grow at the expense of the number of crystallites, and the space between the islands extends gradually. Moreover, portions of the adsorbate desorb from the substrate, resulting in decreasing island density. Among our SEM images, we also observed needle- and belt-like structures lying on the Au substrate. According to

the S-type growth model [16], these structures result from homogeneous nucleation, i.e., the PTCDA molecules combined prior to adsorbing on the substrate. Under these circumstances, the adsorbate formed elongated needles through stacking of additional molecules along the needle's axis.

Figs. 1e–h present the PTCDA film morphologies on the Ti-CVD substrate at the same set of temperatures. In this case, we observed that many more of the needle-like structures existed on the Ti-CVD substrate than they did on the Au substrate. The cause of this change in film morphology is very subtle. Herein we suggest two possibilities. First, according to the film growth mechanism, the adsorbate usually diffuses to the step edges of terraces [23]; thus, the substrate morphology plays an important role as a template. In Fig. 1e, we observe a preformed 1D nanostructure having a diameter of 30 nm that looks like a string of beads. After examining the morphology of the pure Ti-CVD substrate with AFM, we realized that this threaded bead structure existed on the Ti-CVD substrate prior to the formation of the PTCDA film, suggesting that the Ti pillar morphology might induce and enhance the formation of 1D nanostructures of PTCDA. The other possibility is that when the Ti film was deposited using $TiCl_4$ as a liquid source precursor, incompletely reacted $TiCl_4$ probably remained on the Ti film; i.e., some of the Ti surface atoms were still bonded to chlorine atoms. Because $TiCl_4$ and $TiCl_3$ are strongly Lewis acidic (electrophilic) groups [24], such units might provide sites for reacting with PTCDA adsorbate molecules. Table 1 displays the trace element concentration of the Ti-CVD substrate, as determined using TXRF spectrometry. We observe indeed the existence of chlorine atoms on the Ti-CVD substrate (ca. 9 at%). Consequently, when depositing PTCDA at high temperature, the presence of reactive Ti–Cl sites might lead to the preference for deposition of PTCDA and form nanofiber structures.

Comparing Figs. 1d and h, which display images of the materials prepared at a temperature at which some of the PTCDA molecules re-evaporated from the substrate ($T_{sub} = 120$ °C), the number of nanostructures present on the Ti-CVD substrate is greater than that on the Au substrate. We ascribe this phenomenon partly to the dianhydride groups of PTCDA bonding more strongly to the reactive Ti substrate than to the inert Au substrate. This observation is consistent with the UPS results reported by Hirose et al. [25,26]

To confirm our assumption that the nanofibers formed relatively easier on the Ti-CVD substrate as a result of the substrate template effect operating in conjunction with the presence of reactive Ti–Cl sites, we used PVD to prepare another Ti substrate to compare its behavior with that of the Ti-CVD substrate. The Ti-CVD and Ti-PVD films both exhibited hexagonal structures, as characterized using grazing incident X-ray diffraction (GID). Figs. 2a and b display topographic SEM images of the PTCDA films, which we deposited simultaneously, at a value of T_{sub} of 100 °C, onto both the Ti-CVD and Ti-PVD substrates. Both substrates are Ti but with distinct PTCDA film morphologies, it reveals that some other factors besides the crystal structure enhance the growth of the PTCDA nanofibers. Figs. 3a and b present the initial morphologies of the Ti-CVD and Ti-PVD substrates, respectively, prior to deposition of PTCDA. The image of the Ti-PVD surface indicates that it had a smooth topography with a root mean square roughness of 1.3 nm, a value that is quite normal for a sputtered metal film. In contrast, the image for the Ti-CVD sample indicates that pillared structures existed, with a root mean square roughness as high as 25.5 nm. Based on the theory that the adsorbate has a greater tendency to diffuse toward and grow along the step edge, we attribute the enhanced growth of the 1D nanostructures on Ti-CVD primarily to its abrupt pillar-shaped morphology. When we deposited PTCDA on the heated Ti-CVD substrate, the mobile adsorbate molecules shifted location to the vicinity of the Ti pillars and grew around them.

The results of the TXRF analyses for both substrates (Table 1) further support our hypotheses. Although we detected chlorine atoms (ca. 9 at.%) on the Ti-CVD substrate, none could be detected on the Ti-PVD substrate. As mentioned previously, $TiCl_x$ species are highly reactive Lewis acids – for example, some are used as Ziegler–Natta catalysts for olefin polymerization [27]. If the reactive Ti–Cl sites of our substrate act as anchor sites of the first set of deposited PTCDA molecules, subsequent

Table 1
The concentration of trace elements on Ti-CVD substrate and Ti-PVD substrate

Element	Ti-CVD substrate concentration ± sigma (10^{10} atoms/cm^2)	Ti-PVD substrate Concentration ± sigma (10^{10} atoms/cm^2)
Ti	673940.55 ± 6619.29	255681.04 ± 2469.12
Cl	60211.44 ± 700.33	Not detected

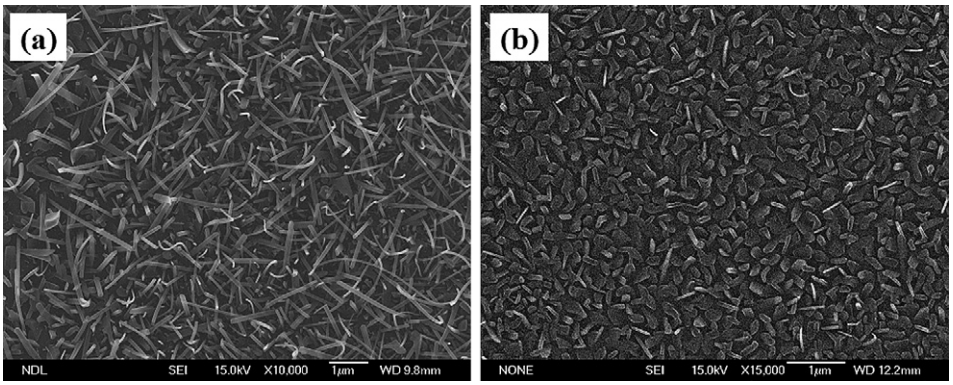

Fig. 2. Top-view SEM images of PTCDA layers deposited on (a) Ti-CVD and (b) Ti-PVD at values of T_{sub} of 100 °C.

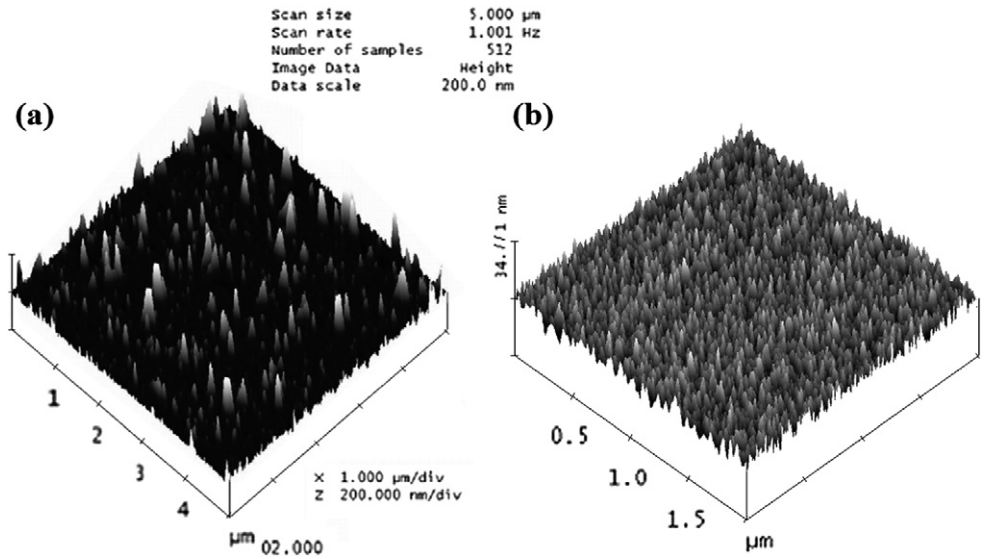

Fig. 3. AFM images of the (a) Ti-CVD (image area: 5×5 μm^2; height: 200 nm) and (b) Ti-PVD (image area: 2×2 μm^2; height: 34.77 nm) substrates.

molecules will deposit upon them through π–π interactions to develop 1D nanostructures. We are presently undertaking further studies to verify the exact details of this reaction mechanism.

Fig. 4 presents side-view SEM images of the PTCDA nanofibers deposited on the Ti-CVD substrate at a value of T_{sub} of 100 °C. The average diameter of these nanofibers was ca. 84 nm, with lengths ranging from 100 nm to 3 μm. The nanofibers stand with angles on the Ti substrate as a result of repulsive forces among nuclei, which led to a parallel-displaced conformation and resulted in tilted columnar structures [28].

Fig. 5a presents an HRTEM image of a single PTCDA nanofiber, having a diameter of 22 nm, that was formed at a value of T_{sub} of 100 °C on the Ti-CVD substrate. In Fig. 5b, the high-magnification image displays fringes that are orientated in short-range order at the edges of the nanofiber, but entangled randomly within the nanofiber. The electron diffraction pattern presented in the inset of Fig. 5a displays only amorphous rings, rather than distinct diffractive spots, suggesting an insignificant degree of crystallinity. In addition, we did not observe any catalyst at the tip of the fiber, similar with previous results of other organic nanofibers [11,13]. Therefore, the growth mechanism is dissimilar to that of carbon nanotubes (CNTs), which require a catalyst surface to enhance the decomposition of the hydrocarbon reactants, forming a super-

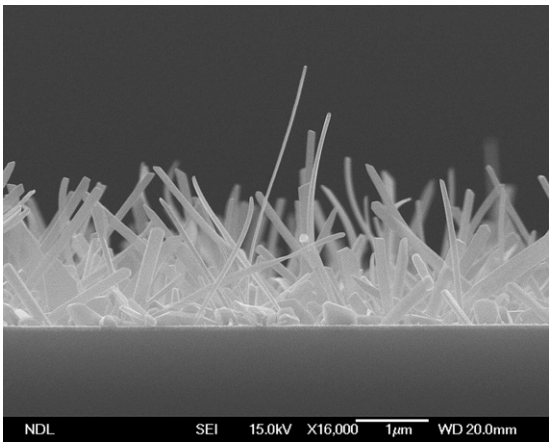

Fig. 4. Side-view SEM images of PTCDA nanofibers deposited on the Ti-CVD substrate at a value of T_{sub} of 100 °C.

saturated solution of carbon and catalyst, which finally precipitates carbon atoms and extrudes the walls [29].

Interestingly, although most of the PTCDA nanofibers were amorphous and included no catalyst, certain nanofibers did contain titanium atoms within them. Fig. 5c presents an image of a PTCDA nanofiber having a diameter of ca. 12 nm. This nanofiber possessed a heterogeneous structure, as indicated by the arrow. When selected area diffraction (SAD) was performed, a distinct diffraction pattern was observed, as shown in the inset of Fig. 5c. We examined this heterogeneous structure further through the use of energy dispersive spectroscopy (EDS), with which we found peaks associated with Ti atoms. Fig. 5d presents a magnified image of the heterogeneous structure, which shows that Ti atoms arranged in an ordered manner within the nanofiber, accompanied by amorphous carbon atoms located around the outer region. This observation further supports our mechanism for the growth of PTCDA nanofibers. Parts of the PTCDA nanostructure grew along the Ti pillars and, in some cases, they grew around these pillars. The highly electronegative chlorine atoms on the Ti surface attract electrons and weaken the bonding between Ti atoms; consequently, some of the chlorine-bound Ti atoms ($TiCl_x$) might desorb from the surface at

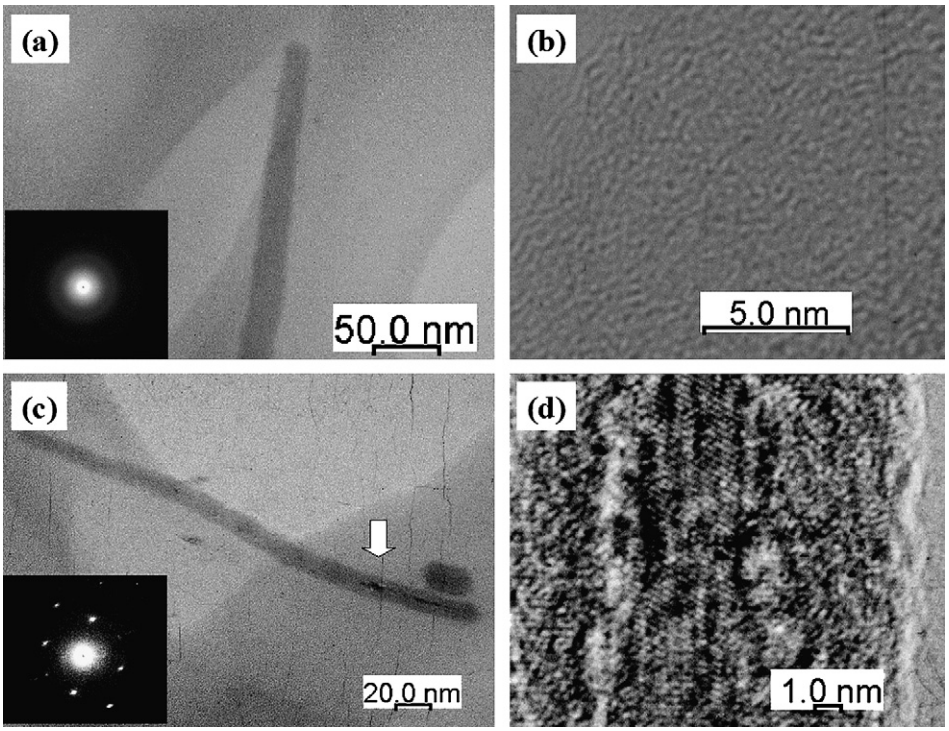

Fig. 5. (a) HRTEM image of a single PTCDA nanofiber formed on the Ti-CVD substrate at a value of T_{sub} of 100 °C. Inset: The corresponding electron diffraction pattern. (b) A magnified image of the nanofiber in (a), displaying its amorphous structure. (c) HRTEM image of a single Ti-included PTCDA nanofiber (diameter: 12 nm). The corresponding electron diffraction pattern in the inset displays Ti atoms within the fiber. (d) Magnified image of the nanofiber in (c), highlighting the heterogeneous region, which exhibits a crystallized structure.

high temperature. Because Ti atoms have a great tendency to react with the anhydride groups of PTCDA [25], desorbed $TiCl_x$ species might react with incoming PTCDA adsorbate units to form Ti-included PTCDA nanofibers.

Field emission characterization of the PTCDA nanofibers synthesized on a heated (100 °C) Ti-CVD substrate was performed under vacuum (5×10^{-6} torr) by placing a cylindrical Cu electrode (diameter: 2.2 mm) at a distance of 100 μm above the surface of the sample. The Cu electrode was connected to the source monitor unit (SMU) of a Keithley 237 instrument, and the titanium substrate beneath the PTCDA nanofibers was grounded. Fig. 6 presents the emission current density (J) as a function of the applied field (E). The turn-on field required for the PTCDA nanofibers to produce a current density of 10 μA/cm^2 was 8 V/μm. The maximum emission current density of 1.3 mA/cm^2 occurred at a potential of 1100 V ($E = 11$ V/μm). This performance is better than that of the CuPc nanofibers that we reported previously [13]. From the point of view of electron injection, the electron affinity (4.6 eV) of PTCDA [30] is close to the work function (4.33 eV) of the Ti substrate [31]; thus, electrons are able to transfer from the Ti substrate to the PTCDA nanofibers much more readily than they could from an Au substrate (5.1 eV) to CuPc nanofibers (3.1 eV). Furthermore, the strong bonding between the Ti substrate and the dianhydride groups of PTCDA molecules provides a better interface for electron injection [25].

The Fowler–Nordheim (FN) theory is most commonly used to model the emission of cold electrons from a conductor under a strong field [32]. By plotting $\ln(J/E^2)$ versus $1/E$, one can obtain a straight line, the slope of which can be used to deduce the field enhancement factor (β) [33]. The inset of Fig. 6 indicates that the plot of $\ln(J/E^2)$ versus $1/E$ is a straight line, implying that the field emission from these nanofibers follows FN theory. From the values of the work function of bulk PTCDA (4.6 eV) and the slope of the fitted line (−64.21 V/μm), we calculated the field enhancement factor β of the PTCDA nanofibers to be 989 cm^{-1}. This value is smaller than determined for a CNT film (1000–3000 cm^{-1} for a 125-μm inter-electrode distance) [34], presumably because of the different length-to-radius (L/r) ratios of the 1D nanostructure, as has been discussed elsewhere [9]. As compared with similar π-stacked organic 1D nanostructure, AlQ_3 nanowires, the field enhancement factor of the PTCDA nanofibers is higher than the value of AlQ_3 nanowires ($\beta = 275$ cm^{-1}) [9]. Although the L/r ratio of the AlQ_3 nanowires ($L/r = 5.5$ μm/20 nm = 275) was higher than that of the PTCDA nanofibers ($L/r = 2.2$ μm/84 nm = 26), the lower work function of AlQ_3 (3.0 eV) relative to that of PTCDA (4.6 eV) limits the deduced value of β according to the formula $\beta = B\phi^{3/2}/\text{slope}$, where $B = 6.83 \times 10^9$ V m^{-1} eV$^{-3/2}$ [8,33]. This result reveals that the geometric shape and intrinsic properties of the emitter both influence the field enhancement effect.

Fig. 7 displays the emission current stability of the PTCDA nanofibers when biased at 1000 V ($E = 10$ V/μm) for 1600 s. The mean current density was ca. 0.5 mA/cm^2 with a perturbation of less than

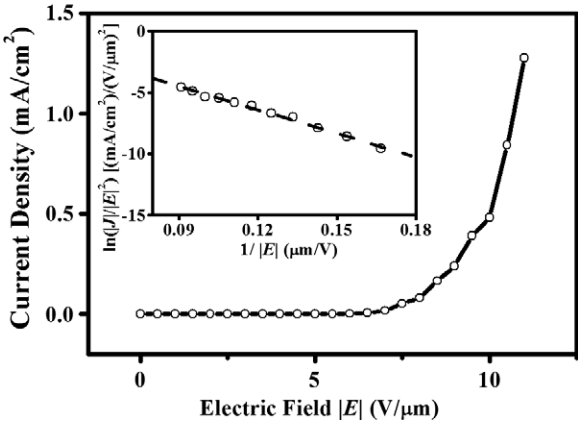

Fig. 6. Field emission $J - E$ curve of the PTCDA nanofibers. Inset: Corresponding FN plot.

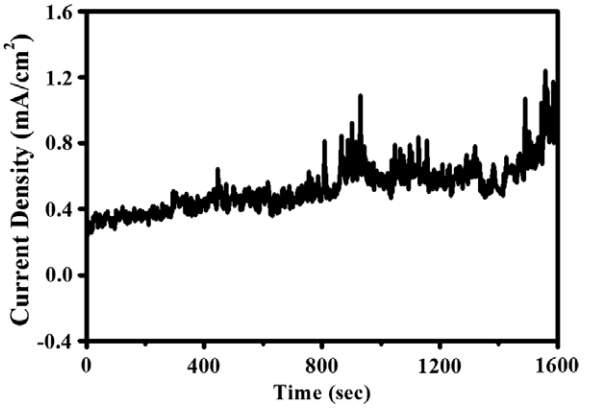

Fig. 7. Emission current of the PTCDA nanofibers plotted at a constant voltage.

one order of magnitude. The increasing tendency of emission current might result from the training effect [35,36] that some contaminants have been expelled after biasing the nanofibers for a period of time. The field emission current did not decay during the stability measurements, demonstrating that the PTCDA organic nanofibers is suitable for applications as electron-emitting devices.

4. Conclusions

In this study, we observed the temperature-induced morphological changes that occurred to PTCDA on Au, Ti-PVD, and Ti-CVD substrates. Owing to the presence of pillared Ti structures and Ti–Cl reactive sites, PTCDA nanofibers grew much more readily on the Ti-CVD substrate than on the Au and Ti-PVD substrates. A stable emission current was measured when the PTCDA nanofibers were biased under vacuum. The turn-on field required to produce a current density of 10 $\mu A/cm^2$ was 8 V/μm. The maximum emission current density was 1.3 mA/cm^2, measured at $E = 11$ V/μm. From the slope of the straight line obtained after plotting $\ln(J/E^2)$ versus $1/E$, we calculated the field enhancement factor β to be ca. 989. These results demonstrate an alternative application of PTCDA as an electron-emitting device and open up an interesting area of study of the anisotropic carrier transfer in 1D organic nanostructure.

Acknowledgements

We thank the National Science Council of the Republic of China for supporting this research financially under Contract No. NSC 95-2221-E-009-121. We are also grateful for the technical support provided by the National Nano Device Laboratories.

References

[1] S.R. Forrest, Chem. Rev. 97 (1997) 1793.
[2] M. Eremtchenko, J.A. Schaefer, F.S. Tautz, Nature 425 (2003) 602.
[3] N. Karl, J. Marktanner, R. Stehle, W. Warta, Synth. Met. 41–43 (1991) 2473.
[4] W. Warta, N. Karl, Phys. Rev. B 32 (1985) 1172.
[5] C.W. Tang, S.A. VanSlyke, Appl. Phys. Lett. 51 (1987) 913.
[6] H.P. Wagner, A. DeSilva, Phys. Rev. B 70 (2004) 235201.
[7] A. Dodabalapur, H.E. Katz, L. Torsi, Adv. Mater. 8 (1996) 853.
[8] K. Triyana, T. Yasuda, K. Fujita, T. Tsutsui, Thin Solid Films 477 (2005) 198.
[9] J.J. Chiu, C.C. Kei, T.P. Perng, W.S. Wang, Adv. Mater. 15 (2003) 1361.
[10] H. Liu, Q. Zhao, Y. Li, Y. Liu, F. Lu, J. Zhuang, S. Wang, L. Jiang, D. Zhu, D. Yu, L. Chi, J. Am. Chem. Soc. 127 (2005) 1120.
[11] S.C. Suen, W.T. Whang, B.W. Wu, Y.F. Lai, Appl. Phys. Lett. 84 (2004) 3157.
[12] H. Liu, Y. Li, S. Xiao, H. Gan, T. Jiu, H. Li, L. Jiang, D. Zhu, D. Yu, B. Xiang, Y. Chen, J. Am. Chem. Soc. 125 (2003) 10794.
[13] S.C. Suen, W.T. Whang, F.J. Hou, B.T. Dai, Org. Electron. 7 (2006) 428.
[14] B. Krause, A.C. Dürr, K. Ritley, F. Schreiber, H. Dosch, D. Smilgies, Phys. Rev. B 66 (2002) 235404.
[15] B. Krause, A.C. Dürr, F. Schreiber, H. Dosch, O.H. Seeck, J. Chem. Phys. 119 (2003) 3429.
[16] M. Möbus, N. Karl, J. Crystal Growth 116 (1992) 495.
[17] M. Stöhr, M. Gabriel, R. Möller, Surf. Sci. 507–510 (2002) 330.
[18] L. Chkoda, M. Schneider, V. Shklover, L. Kilian, M. Sokolowski, C. Heske, E. Umbach, Chem. Phys. Lett. 371 (2003) 548.
[19] Th. Wagner, A. Bannani, C. Bobisch, H. Karacuban, M. Stöhr, R. Gabriel, R. Möller, Org. Electron. 5 (2004) 35.
[20] J. Hu, M. Ameen, G. Leusink, D. Webb, J.T. Hillman, Thin Solid Films 308–309 (1997) 589.
[21] P. Fenter, F. Schreiber, L. Zhou, P. Eisenberger, S.R. Forrest, Phys. Rev. B 56 (1997) 3046.
[22] B. Krause, F. Schreiber, H. Dosch, A. Pimpinelli, O.H. Seeck, Europhys. Lett. 65 (2004) 372.
[23] F. Schreiber, Phys. Status Solidi 201 (2004) 1037.
[24] J. McMurry, third ed.Organic Chemistry, Brooks/Cole, 1992, p. 55.
[25] Y. Hirose, A. Kahn, V. Aristov, P. Soukiassian, V. Bulovic, S.R. Forrest, Phys. Rev. B 54 (1996) 13748.
[26] Y. Hirose, A. Kahn, V. Aristov, P. Soukiassian, Appl. Phys. Lett. 68 (1996) 217.
[27] A.F. Hill, Organotransition Metal Chemistry, Wiley-Inter-Science, New York, 2002, p. 136.
[28] J.D. Wright, Molecular Crystals, second ed., Cambridge University Press, 1995, p. 22.
[29] V. Vinciguerra, F. Buonocore, G. Panzera, L. Occhipinti, Nanotechnology 14 (2003) 655.
[30] A. Rajagopal, C.I. Wu, A. Kahn, J. Appl. Phys. 83 (1998) 2649.
[31] H. Wu, S.R. Desai, L.S. Wang, Phys. Rev. Lett. 76 (1996) 212.
[32] R.H. Fowler, L. Nordheim, Proc. Royal Soc. London Ser. A 119 (1928) 626.
[33] V.V. Zhirnov, C. Lizzul-Rinne, G.J. Wojak, R.C. Sanwald, J.J. Hren, J. Vac. Sci. Technol. B 19 (2001) 87.
[34] J.M. Bonard, J.P. Salvetat, T. Stöckli, W.A. de Heer, L. Forró, A. Châtelain, Appl. Phys. Lett. 73 (1998) 918.
[35] J.M. Bonard, N. Weiss, H. kind, T. Stöckli, L. Forró, K. Kern, A. Châtelain, Adv. Mater. 13 (2001) 184.
[36] S.K. Patra, G.M. Rao, J. Appl. Phys. 100 (2006) 024319.